

Robust multi-objective optimization under multiple-uncertainties using CM-ROPAR approach: case study of the water resources allocation in the Huaihe River Basin

Jitao Zhang^{1,2,3}, Dimitri Solomatine^{2,3,4}, Zengchuan Dong¹

¹College of Hydrology and water resources, Hohai University; Nanjing, 210000, China.

²Water Resources Section, Delft University of Technology; Delft, 2628 CD, Netherlands.

³IHE Delft Institute for Water Education; Delft, 2628 AX, Netherlands

⁴Water Problems Institute of RAS, Moscow 119333, Russia

Correspondence to: Zengchuan Dong (zcdong@hhu.edu.cn)

Abstract. Water resources managers need to make decisions in a constantly changing environment because the data relating to water resources is uncertain and imprecise. The Robust Optimization and Probabilistic Analysis of Robustness (ROPAR) algorithm is a well-suited tool for dealing with uncertainty. Still, the failure to consider multiple uncertainties and multi-objective robustness hinder the application of the ROPAR algorithm to practical problems. This paper proposes a robust optimization and robustness probabilistic analysis method that considers numerous uncertainties and multi-objective robustness for robust water resources allocation under uncertainty. The Copula function is introduced for analyzing the probabilities of different scenarios. The robustness with respect to the two objective functions is analyzed separately, and the Pareto frontier of robustness is generated. The relationship between the robustness with respect to the two objective functions is used to evaluate water resources management strategies. Use of the method is illustrated on a case study of water resources allocation in the Huaihe River Basin. The results demonstrate that the method opens a possibility for water managers to make more informed uncertainty-aware decisions.

1. Introduction

Water resources is a natural resource necessary for human survival (Chen et al., 2017) but also a driving force for social and economic development (Dong and Xu, 2019). Due to the increasing population and rapid growth of economy, a contradiction between the supply and demand of water resources is becoming more acute, water quality problems are becoming more prominent, and water resources have gradually become a bottleneck for socio-economic development (Zhuang et al., 2018). This phenomenon is particularly evident in rapidly urbanizing and vital agricultural and industrial production watersheds (Yang et al., 2017). In this category of watersheds, agricultural and industrial production pose a massive challenge to water resource management (WRM) due to accelerated urbanization and rapid socio-economic development (Sun et al., 2019). River basin managers must consider water sources in an integrated manner and decide how to allocate water resources between different water-using sectors and cities within the basin (Xiong et al., 2020).

Multi-objective optimization (MOO) is an effective method for improving water resources allocation

37 (WRA) schemes (Lu et al., 2017; Abdulbaki et al., 2017). MOO can provide decision-makers with WRA
38 options based on their preferences for objectives, which makes it a well-suited decision-making method
39 for WRM. Ashofteh et al. (2013) constructed a bottom-line-based multi-objective optimization model to
40 calculate WRA schemes. Habibi Davijani et al. (2016) presented a multi-objective optimal allocation
41 model of water resources in arid areas based on maximum socioeconomic benefits. However, WRM is
42 not only a multi-stage and multi-objective problem but also a complex problem involving uncertainties
43 and risk management (Yu and Lu, 2018). WRM departments often need to face decision challenges under
44 uncertain conditions (Hassanzadeh et al., 2016; Ren et al., 2019). Climate change and human activities
45 have led to an increase in uncertainties in rainfall and water demand in the basin and hence to uncertainty
46 in managing water resource systems (Jin et al., 2020; Ma et al., 2020; Zhu et al., 2019). Uncertain factors
47 may lead to the risk of water shortage in the basin, so the existing WRA schemes may not be longer
48 applicable (Keath and Brown, 2009). Therefore, it is important to study WRA under uncertainty.

49 Previously, several methods were introduced to analyze uncertainty in WRM. Scenario building and
50 analysis is regarded as an effective method for considering possible future events and analyzing future
51 uncertainties (Zeng et al., 2019). The fuzzy logic theory is one of the methods to deal with uncertainty,
52 which describes uncertainty by fuzzifying the decision variables (Nikoo et al., 2013). Two-stage
53 stochastic programming (TSP) is also an available planning method in optimization under uncertainty
54 (Li et al., 2020). However, these approaches do not explicitly evaluate the robustness of the WRA options,
55 although they take into account the uncertainties in WRA.

56 Robust multi-objective optimization (RMOO) is an effective method for forming robust WRA schemes.
57 In relation to water, RMOO was actively applied in the field of water supply system (Kapelan et al., 2005;
58 Kapelan et al., 2006). In the last decade, RMOO has been gradually applied to other areas of WRM.
59 Yazdi et al. (2015) and Kang and Lansey (2013) applied robust optimization to design wastewater pipes
60 by considering uncertainties such as climate change, urbanization, and population change. Marchi et al.
61 (2016) formed stormwater harvesting schemes under variable climate conditions using RMOO. It should
62 be pointed out however, that in the mentioned approaches the robustness is often “hidden” into the
63 objective function or constraints and then a common MOO problem is solved that forms a single Pareto
64 front. This is indeed an effective method to create solution set which in a certain sense is robust. However,
65 this approach does not explicitly show the relationship between the solution and the uncertainty variables,
66 which prevents the decision-maker from clearly understanding the impact of uncertainty, which can
67 influence the decision. To answer this limitation, the procedure “Robust Optimization and Probabilistic
68 Analysis of Robustness” (ROPAR) has been developed and presented first in (Solomatine, 2012). The
69 method will generate multiple Pareto fronts, each corresponding to a sample of uncertain variables so
70 that the statistical characteristics of the uncertainty of the solution can be analyzed. The ROPAR has been
71 applied in the design of urban stormwater drainage pipes (Solomatine and Marquez-Calvo, 2019) and for
72 water quality management in water distribution (Marquez Calvo et al., 2019; Quintiliani et al., 2019).

73 To the best of our knowledge, the presented versions of the ROPAR methodology have the following
74 limitations: (1) ROPAR method has not been applied to the field of WRA; (2) ROPAR method only
75 considers the single source of uncertainty: if there are two sources, then the joint probability of these
76 sources needs to be considered; (3) ROPAR method only analyses the variability of one objective under
77 conditions where the other objective function level is fixed. Although the ROPAR method can provide
78 decision-makers with a robust solution under certain conditions, it does not take into account the
79 relationship between the two objective functions.

80

81

82 Based on the above analysis, although the ROPAR method has proven to be suitable for dealing
83 with uncertainty, it still needs improvement. In this study, we propose a Copula-Multi-objective Robust
84 Optimization and Probabilistic Analysis of Robustness (CM-ROPAR) procedure under multiple
85 uncertainties for WRA. The proposed new procedure of the ROPAR-family considers the joint
86 probability distribution of uncertainties (in this case, inflows) and enables decision-makers to check the
87 robustness of the two objective functions separately.

88 The following text is structured as follows. First, the Chapter 2 presents the methodology of the
89 paper. It mainly includes the method of Copula function, the method of CM-ROPAR algorithm, the
90 definition of robustness and the construction of water resources allocation model. Then, the Chapter 3
91 introduces the overview of the study area. Then, the Chapter 4 introduces the application examples of
92 CM-ROPAR algorithm, and this paper is an example of water resources allocation of Huaihe River Basin.
93 Finally, the last Chapter introduces the conclusion of the paper.

94

95 2. Methodology

96 2.1 Method of Copula Function

97 Sklar proposed Copula theory in 1959, in which he decomposed an N-dimensional Joint Distribution
98 Function (JDF) into a Copula function and N Marginal Distribution Functions (MDF), which are not
99 required to be the same distribution for N variables and can be used to describe the correlation between
100 arbitrary variables. Nelsen discussed the basic properties and some of the main applications of Copula
101 functions in 1999 (Nelsen et al., 2008). Copula function is the function that connects the JDF with their
102 respective MDF. Copula functions can be expressed as:

$$103 C_{\theta}(u_1, u_2 \dots u_n) = C_{\theta}[F_1(x_1), F_2(x_2) \dots F_n(x_n)] \quad (1)$$

104 where $x_1, x_2 \dots x_n$ are random vectors, $u_1 = F_1(x_1), u_2 = F_2(x_2) \dots u_n = F_n(x_n)$ are MDF of
105 the random vectors, θ is the parameter or the parameter vector of copula function.

106 The basic copula functions are mainly classified into Archimedean, elliptic, and quadratic types.
107 Among them, Archimedean Copula functions have been widely applied in the field of
108 hydrology (Salvadori et al., 2007). The Archimedean Copula multidimensional joint distribution models
109 are the following:

110 (1) GH-Copula joint distribution model

$$111 C_{\theta}(u_1, u_2 \dots u_n) = \exp \left[-(\sum_{i=1}^n (-\ln u_i)^{\theta})^{\frac{1}{\theta}} \right] \quad (\theta > 1), \quad (2)$$

112 (2) Clayton Copula joint distribution model

$$113 C_{\theta}(u_1, u_2 \dots u_n) = [1 + \sum_{i=1}^n (u_i^{-\theta} - 1)]^{-\frac{1}{\theta}} \quad (\theta \in [-1, \infty) \setminus \{0\}), \quad (3)$$

114 (3) Frank Copula joint distribution model

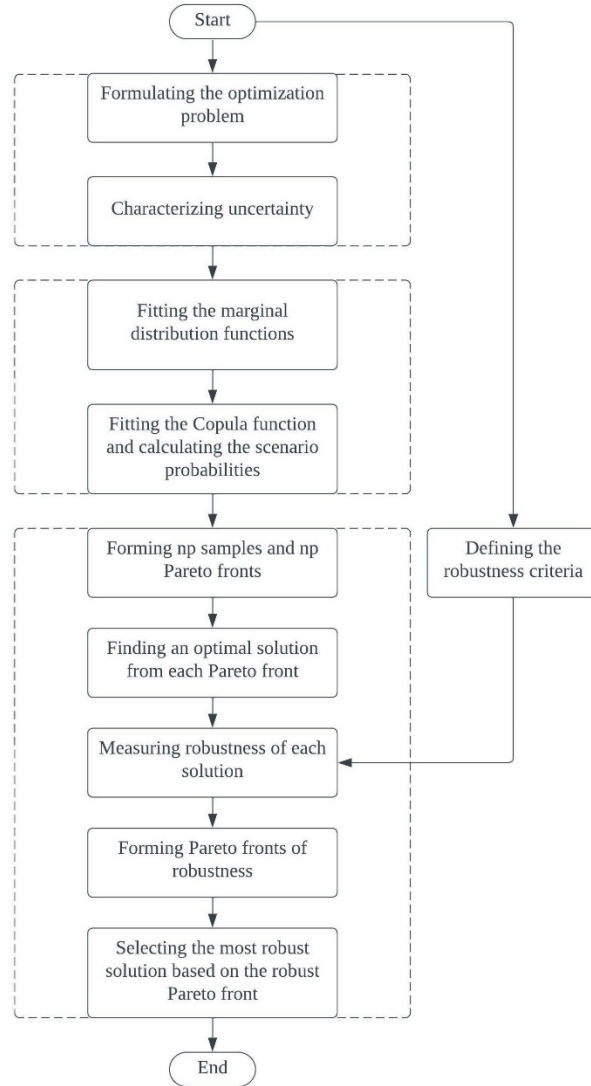
$$115 C_{\theta}(u_1, u_2 \dots u_n) = -\frac{1}{\theta} \ln \left[1 + \frac{\prod_{i=1}^n (e^{-\theta u_i} - 1)}{(e^{-\theta} - 1)^{n-1}} \right] \quad (\theta \in R \setminus \{0\}), \quad (4)$$

116 In a river basin, there may be different drought or wet conditions between different intervals of
117 inflow, so the probability of drought and wet encounters between different intervals of inflow needs to
118 be investigated. According to the analysis in Section 2.1, it is known that Copula function can be used to

119 construct the multivariate joint distribution function. Therefore, this paper adopts Copula function theory
120 to construct the joint distribution and analyze the drought and wet encounter probability. The steps of
121 Copula function-based wet-dry encounter analysis are as follows: 1. Fit and Select the MDF. The widely
122 applied probability distribution functions are mainly Pearson type 3 distribution (P-III), T-distribution,
123 Normal distribution, etc. **MDF can be fitted by Maximum Likelihood Estimation method (MLE method)**
124 **and the goodness-of-fit test can be performed by the Kolmogorov-Smirnov test (K-S test) and the Root**
125 **Mean Square Error value (RMSE value).** 2. Fit and Select Copula distribution function. Based on the
126 MDF fitted in the first step, construct the Copula function and select the fitted Copula function by AIC
127 and BIC criteria. 3. Calculate the probability of a dry and wet encounters between different interval
128 inflows.
129

130 2.2 Method of CM-ROPAR

131 The basic flow of CM-ROPAR algorithm is shown in Figure 1. Firstly, the multi-objective optimization
132 problem is defined and the uncertainty variables are clarified; secondly, the Copula function is used to
133 analyze the relationship between the two sources of uncertainty; and finally, through sampling and multi-
134 objective optimization calculations, the robustness of each solution is identified and the one with the
135 most comprehensive robustness is selected.
136
137



138

139 **Figure 1.** Flowchart of CM-ROPAR.

140

141 The specific process of optimal water allocation under runoff uncertainty based on MROPAR algorithm
 142 is as follows.

143 **Part 1** (Analyzing the wet-dry encounters)

144 1. Analyze the inflow wet and dry encounters. If the basin has k inflows, then there are 3^k wet-
 145 dry scenarios. For example, suppose there is one inflow in the upper and one in the middle reaches of the
 146 basin. In that case, there are 9 scenarios: wet-medium, wet-wet, medium-wet, medium-medium, medium-
 147 dry, dry-wet, dry-medium, and dry-dry.

148 2. Choose a scenario from 1 to 3^k .

149 **Part 2** (Sampling-Inflow)

150 3. Based on the recorded annual inflow data Q , it is assumed that Q is not a definite value but

151
$$Q = i_{uncertainty} * Q, \tag{5}$$

152
$$i_{uncertainty} \sim N(\mu, \sigma^2), \tag{6}$$

153 where $i_{uncertainty}$ follows a normal distribution.

154 4. For $i = 1 \dots np$ do

155 5. Sample u (inflow). As mentioned before, the uncertainty variable is obtained from the normal

156 distribution $N(\mu, \sigma^2)$. Assuming that the uncertainty variable follows $N(1,0.0025)$, this represents that
 157 a 99.74% probability of the uncertainty variable falling within the interval $[0.85, 1.15]$ and the inflow
 158 sample falling within the interval $[0.85 * Q, 1.15 * Q]$.

159 **Part 3** (Forming the optimal solution set through np Pareto fronts)

160 7. Select an ideal solution (IS) in each Pareto front F_r based on the distance to the origin point,
 161 forming the optimal solution set (set S).

162 **Part 4** (Evaluate the robustness of each solution)

163 8. Select a solution s_i ($i = 1 \dots np$) from the solution set S .

164 9. Cast the inflow case u_r ($r = 1 \dots np$) into s_i and calculate $P_r(u_r, s_i)$ and $WD_r(u_r, s_i)$,
 165 respectively, to form 1200 values of P_r and WD_r ($r = 1 \dots np$).

166 10. Select the robustness evaluation criteria, $RC1, RC2, RC3, RC4$.

167 11. For each s_i ($i = 1 \dots np$), calculate the $RC1, RC2, RC3, RC4$ and SRI corresponding to P_r
 168 and WD_r respectively. Plot the corresponding graphs and find the Pareto front of each graph.

169 12. Find the solution with the highest robustness.

170 End

171 2.3 Defining the robustness criteria

172 According to the general definition of robustness, four common Robustness Criteria (RC) were used in
 173 this study (Beyer and Sendhoff, 2007). These must be minimized to achieve the maximum robustness of
 174 the solution, so the lower the criteria, the higher the robustness.

175 For the four RC , two MOO are implicitly defined, and optimization can be named Two Layer-Multi-
 176 objective optimization of Robustness Criteria (TL-MOORC). It is worth noting that TL-MOORC differs
 177 from the problem's MOO. A one-layer MOORC is a solution that may not be minimized at all four RC
 178 simultaneously. This problem can be solved by aggregating the four RC into one, for example, using a
 179 linear weighted combination. The second layer of MOORC is that for the two objective functions of a
 180 solution, the RC for both objective functions may not be minimized at the same time. Therefore, a trade-
 181 off must be made between the RC for the two objective functions.

182 The first RC is the expected value of each objective function, denoted as $RC1$. It reflects the fact that
 183 we want to find a solution that is good on average across all uncertainties and can be represented by:

$$184 RC1(s) = \int_{N(s,u)} f(s,u) p(u) du, \quad (7)$$

185 Where $p(u)$ is the probability density function of the uncertain variable u ; it is the neighborhood of the
 186 solution s .

187 The second RC is the 'worst case' (or 'minimax' case), denoted as $RC2$. This RC is related to
 188 robustness because we want to find a solution s such that the value of each objective function in the
 189 worst case is the minimum possible. It can be presented as follows:

$$190 RC2(s) = \min \left(\max_{N(s,u)} (f(s,u)) \right), \quad (8)$$

191 The third RC is the 'standard deviation' of each objective function, denoted as $RC3$. $RC3$
 192 is related to the robustness of each objective function because we want to find a solution s such that
 193 the value of the objective function would not vary too much due to uncertainty. It can be expressed as
 194 follows:

$$195 RC3(s) = \sqrt{\int_{N(s,u)} (f(s,u) - f(u))^2 p(u) du}, \quad (9)$$

196 The fourth RC is the "probabilistic threshold", denoted as $RC4$. We want to find a solution s that

197 minimizes the probability that the objective function is higher than the threshold of interest q . This
 198 criterion is usually associated with the reliability of the system. It can be expressed as follows:

$$199 \quad RC4(s) = Pr(f(s, u) > q|s), \quad (10)$$

200 In order to evaluate the integrated robustness of the water resources allocation scheme, the weighted
 201 sum of the four Normalized RC ($NRCi$) in this study was used as the integrated robustness criteria. In
 202 this study, we consider that the four RC to be of equal importance, so all four indicators are given a
 203 weight of $\frac{1}{4}$.

$$204 \quad SRI = \frac{1}{4}NRC1 + \frac{1}{4}NRC2 + \frac{1}{4}NRC3 + \frac{1}{4}NRC4, \quad (11)$$

205 (of course, other ways of aggregation can be considered as well.)

206 2.4 Construction of WRA Model

207 Objective function

208 (1) Social Goals: Water Deficit (WD)

$$209 \quad \min f_1(Q) = \sum_{j=1}^J \sum_{k=1}^K \left(\frac{D_{jk} - \sum_{t=1}^T \sum_{i=1}^I Q_{ijkt}}{D_{jk}} \right)^2, \quad (12)$$

210 Where D_{jk} denotes the water demand of the water consumption department k of the city j . Q_{ijkt} is the
 211 water supply quantity of water source i to water consumption department k of the city j in the period
 212 t .

213 (2) Ecological goals: Pollution (P)

$$214 \quad \min f_2(Q) = \sum_{j=1}^J \sum_{k=1}^K d_{jk} p_{jk} \sum_{i=1}^I \sum_{t=1}^T Q_{ijkt}, \quad (13)$$

215 Where d_{jk} denotes the representative pollutant discharge per unit of wastewater of the water department
 216 k of calculation unit j (ton/m³) and p_{jk} represents the sewage discharge coefficient of the water
 217 consumption department of calculation unit. Discharge coefficient of water consumption department k
 218 of calculation unit j . Q_{ijkt} is the water supply quantity of water source i to water consumption
 219 department k of calculation unit j in the period t .

220 Constraints

221 (1) Water demand constraint

$$222 \quad \sum_{i=1}^I \sum_{t=1}^T Q_{ijkt} \leq D_{jk}, \quad (14)$$

223 (2) Water supply capacity constraint

$$224 \quad \sum_{k=1}^K \sum_{j=1}^J \sum_{t=1}^T Q_{ijkt} \leq U_i, \quad (15)$$

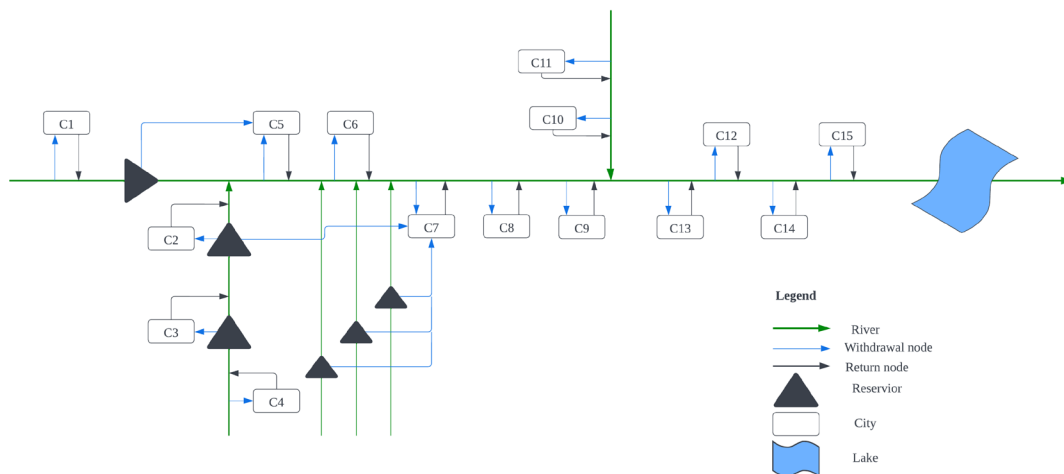
225 (3) Water Resources Constraint

$$226 \quad \sum_{j=1}^J \sum_{k=1}^K Q_{ijkt} \leq WR_i, \quad (16)$$

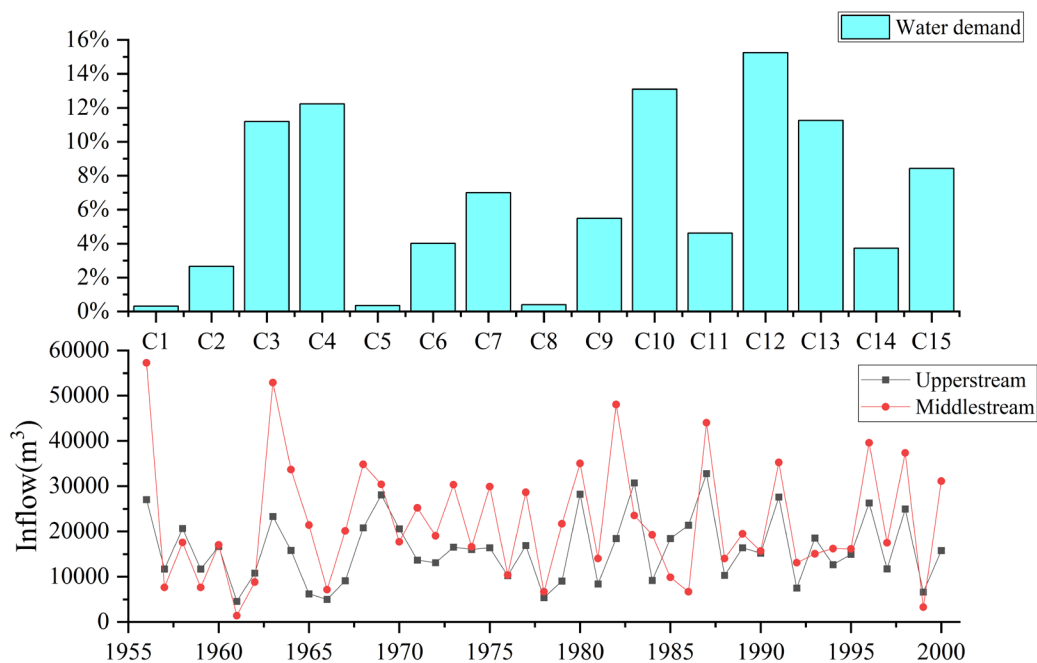
227 3. Study Area Overview

228 The Huaihe River Basin is located in the eastern part of China, and as shown in Figure 2, the middle and
 229 upper basin flows through 15 cities of Henan Province and Anhui Province. It is an important agricultural
 230 and industrial production base in China (Xu et al., 2019). As shown in the Figure 3, the inflow of the
 231 Huaihe River Basin varies significantly between different years and between different regions, and the
 232 water demand is uneven among cities. In this study, water demand is calculated by using the quota
 233 method commonly used in the field of water resources. In addition, due to the discharge of pollutants,
 234 the contradiction between supply and demand of water resources in the middle and upper reaches of the

235 Huaihe River Basin has become increasingly fierce. Therefore, it is meaningful to study the optimal
 236 allocation of water resources and propose a robust water resources allocation scheme based on the wet-
 237 dry encounters in the Huaihe River Basin.



238
 239 **Figure 2.** Overview of watershed water supply.



240
 241 **Figure 3.** Water demand proportion and inflow historical data.

242 4. Results and discussion

243 4.1 Identification of marginal distribution functions

244 According to the first part (step 1-2) of the CM-ROPAR process, we need to construct the joint
 245 probability distributions for the upstream and midstream inflow and generate nine inflow scenarios via

246 the Copula function. Therefore, before constructing the JDF, we need to construct the MDF for the
 247 upstream and midstream inflows respectively. As shown in Table 1, based on the K-S test results and
 248 RMSE value, we found that the best-fitting distributions for the upstream and midstream were the
 249 Weibull and P-III distributions, respectively.

250

251 **Table 1.** MDF goodness-of-fit test results.

	Distribution type	Upper stream inflow	Middle stream inflow
p-value	Normal	0.3341	0.8637
	Log-normal	0.5175	0.5703
	P-III	0.7674	0.7599
	Weibull	0.5758	0.9658
	Rayleigh	0.6123	0.2173
D-value	Normal	0.13721	0.086144
	Lognormal	0.11821	0.1152
	P-III	0.0958	0.0965
	Weibull	0.1129	0.0708
	Rayleigh	0.1096	0.1533
RMSE	Normal	0.0345	0.0522
	Lognormal	0.1391	0.1152
	P-III	0.0306	0.0358
	Weibull	0.0929	0.0306
	Rayleigh	0.0529	0.1736

252

253 4.2 Analysis of upstream and midstream dry and wet encounters

254 The optimal Copula function is selected by comparing the Akaike information criterion (AIC) and the
 255 Bayesian information criterion (BIC), AIC and BIC values in Table 2. It can be concluded that the joint
 256 distribution function of the upper and middle reaches of the Huaihe River Basin is consistent with the
 257 joint distribution of the Clayton Copula function.

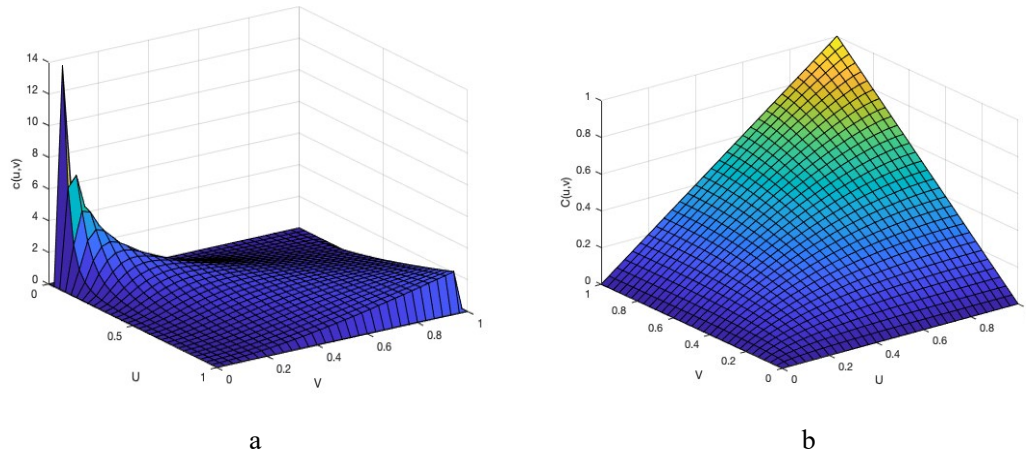
258

259 **Table 2.** AIC and BIC values for Copula functions.

	Gaussian	t	Clayton	Gumbel	Frank
AIC	-20.86	-18.34	-22.69	-12.47	-20.03
BIC	-19.06	-14.73	-20.88	-10.67	-18.22

260

261 Substituting the multi-year annual inflow for the upper and middle reaches of the Huaihe River Basin
 262 into the Clayton Copula function, respectively, the following results were obtained.



263 **Figure 4.** Clayton Copula function.

264

265 As shown in Figure 4, the joint distribution of the annual incoming water in the upper and middle reaches
 266 of the Huaihe River Basin has symmetry. In addition, the joint distribution of annual water in the upper
 267 and middle reaches has a tail correlation, which indicates a higher probability of simultaneous wetness
 268 or drought in the upper and middle reaches.

269

270 **Table 3.** The probabilities of 9 scenarios.

Wet and Dry encounters/%		Upstream		
		Wet	Medium	Dry
Middlestream	Wet	27.7	7.8	5.3
	Medium	11.6	6.5	4.6
	Dry	4.6	7.8	24.1

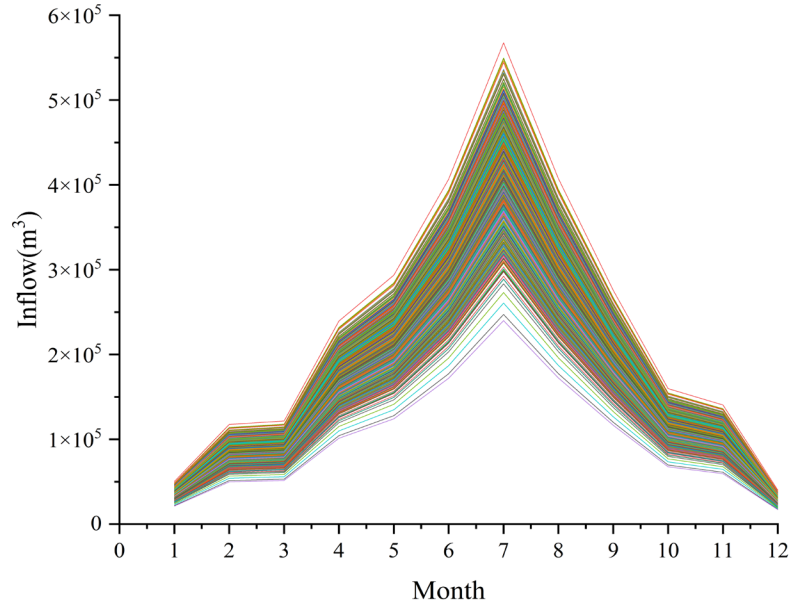
271

272 As shown in Table 3, the probability of drought-wetness synchronization in the upper and middle reaches
 273 of the Huaihe River Basin is 58.3%, while the probability of asynchrony is 41.7%. The former is 16.6%
 274 higher than the latter, indicating that the upper and middle reaches are less able to complement each other.
 275 The joint distribution has a maximum probability of 27.7% that the upstream and midstream are both
 276 wet, and the risk of water scarcity is minimal under this scenario. The joint distribution has the second-
 277 highest probability of both upstream and midstream being dry at 24.1%, with the highest risk of water
 278 scarcity under this scenario.

279 4.3 Considering solutions for the uncertainty of inflow through MROPAR

280 In this study the situation when the upper and middle reaches are both wet is considered as a case study.
 281 For deterministic optimization we opted for the NSGA-II algorithm, which is widely used and has good
 282 historical performance (Reed et al., 2013). Inflow uncertainty is modelled by sampling 1200 inflows, as
 283 shown in Figure 5. In this study, NSGA- II algorithm is used for multi-objective function solving. For
 284 algorithm parameterization, the population size is 100, generation is 1000, cross rate is 0.9 and mutate
 285 rate is 0.2.

286



287

288

Figure 5. Inflow samples.

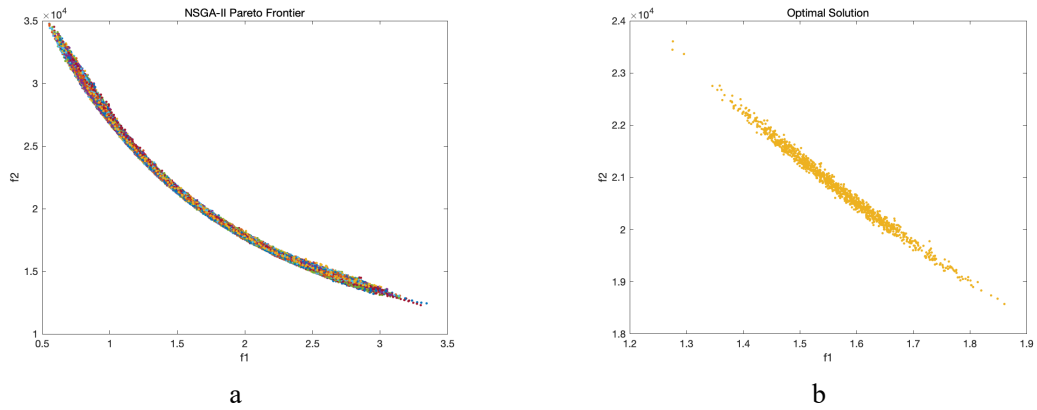
289

290

Figure 6(a) shows that 1200 Pareto fronts calculated for each sampled inflow, through steps 3-6 of CM-ROPAR. Figure 6(b) shows 1200 ideal solutions s , selected based on their distance to the ideal solution (step 7 of CM-ROPAR).

291

292



293

Figure 6. a: 1200 Pareto fronts (f1: water deficit; f2: pollution) and b: 1200 ideal solutions (f1: water deficit; f2: pollution) selected based on their distance to the ideal solution.

294

295

4.4 Assessing robustness of the solutions found by CM-ROPAR

296

Four robustness criteria are calculated for each solution s in the solution set S . Given the solution s to be evaluated, it is necessary to calculate $WD(s, IF_r)(r = 1 \dots np)$ and $P(s, IF_r)(r = 1 \dots np)$ in order to calculate the four robustness criteria, where IF_r is the $rt\hat{k}$ sample of inflow. r depends on the number of samples; in this study, 1200 samples were taken, so np is 1200.

299

300

As shown in Table 4 and Figure 7, $RC1, RC2, RC3, RC4$ and SRI for WD and P can be calculated for each solution in S , and the solutions corresponding to the smallest value in each RCi and the solutions corresponding to the smallest value in SRI can be identified, respectively. In addition, we also feed 1200 samples to the deterministic solution and calculate $RC1, RC2, RC3, RC4$ and SRI for WD and P .

301

302

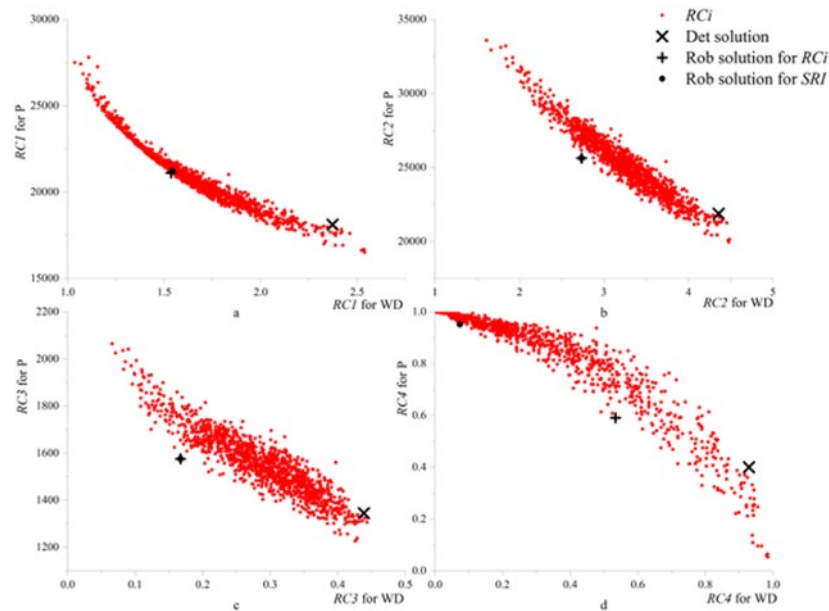
303

304

305

Table 4. Optimal solution numbers for different robustness criteria.

	$RC1$	$RC2$	$RC3$	$RC4$	SRI
WD	535	361	361	361	361
P	876	876	876	876	876
IS	629	84	84	915	84



307

308 **Figure 7.** Performance of the robustness of solutions (a: $RC1$, b: $RC2$, c: $RC3$, d: $RC4$): robust model
 309 solutions (red dots), deterministic model solution (black \times), solution closest to origin for RCi (black +),
 310 solution closest to origin for SRI (black dot). The horizontal axis represents the performance of the
 311 robustness for WD . The vertical axis represents the robustness performance for P .

312

313 Figure 7 shows the performance of 1200 robust model solutions (red dots) and one deterministic model
 314 solution (black \times), for the four robustness criteria. From Figure 7, four Pareto fronts can also be found,
 315 which indicate the competitive relationship between water deficit and pollution emissions for each
 316 robustness criterion dimension. As shown in Figure 7(a), we can observe an interesting phenomenon that
 317 the left-most extreme solution (red dot) has the smallest robustness index $RC1$ for water deficit, but the
 318 highest robustness index $RC1$ for pollution; the right-most extreme solution (red dot) has the largest
 319 robustness index $RC1$ for water deficit, but the smallest robustness index $RC1$ for pollution. Similarly,
 320 this phenomenon can be also observed for the robustness criteria $RC2$, $RC3$, and $RC4$. More
 321 importantly, as shown in Table 4, the extreme solutions and the solutions closest to the origin point may
 322 differ for different robustness criteria. Specifically, for $RC1$, solution No. 535 is the most robust for
 323 water deficit, and solution No. 876 is the most robust for pollution; for $RC2$, $RC3$, and $RC4$, the most
 324 robust solution for water deficit is solution No. 361, and the most robust solution for pollution is solution
 325 No. 876.

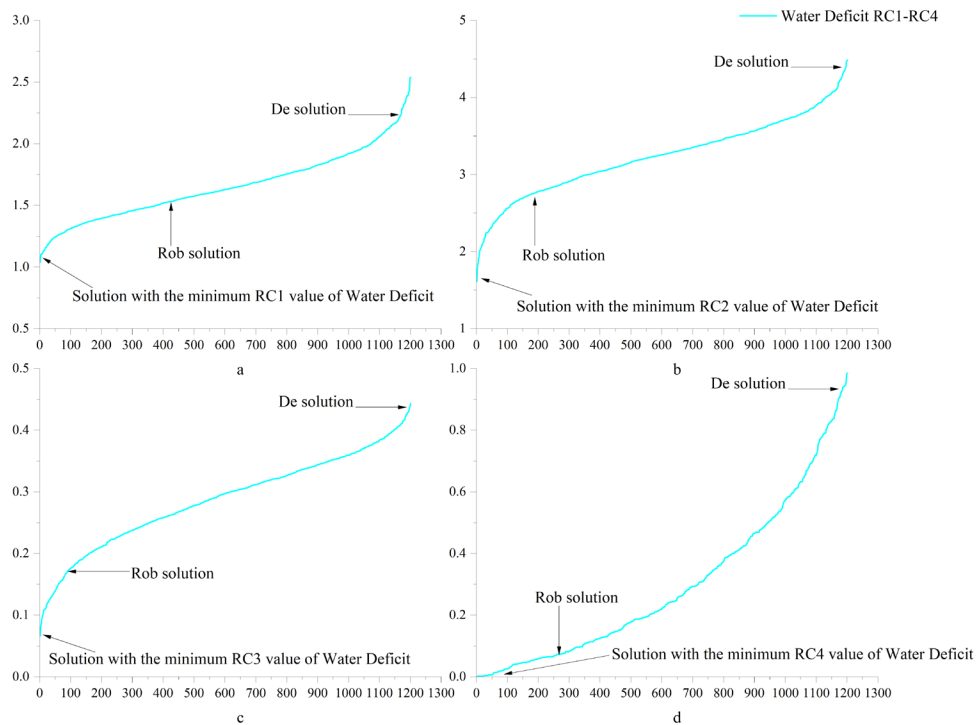
326

327 Because there are many non-inferior solutions in the Pareto frontier, the decision-makers must
 328 choose among them. The decision-makers need not only to choose among the non-inferior solutions but
 329 also to evaluate the trade-off between different robustness criteria or to choose the best one by combining
 the criteria. This study takes the distance to the origin as the basis for such choice. As shown in Table 4,

330 for $RC1$, $RC2$, $RC3$, and $RC4$, the closest points to the origin are solution No. 629, solution No. 84,
 331 and solution No. 915, respectively.

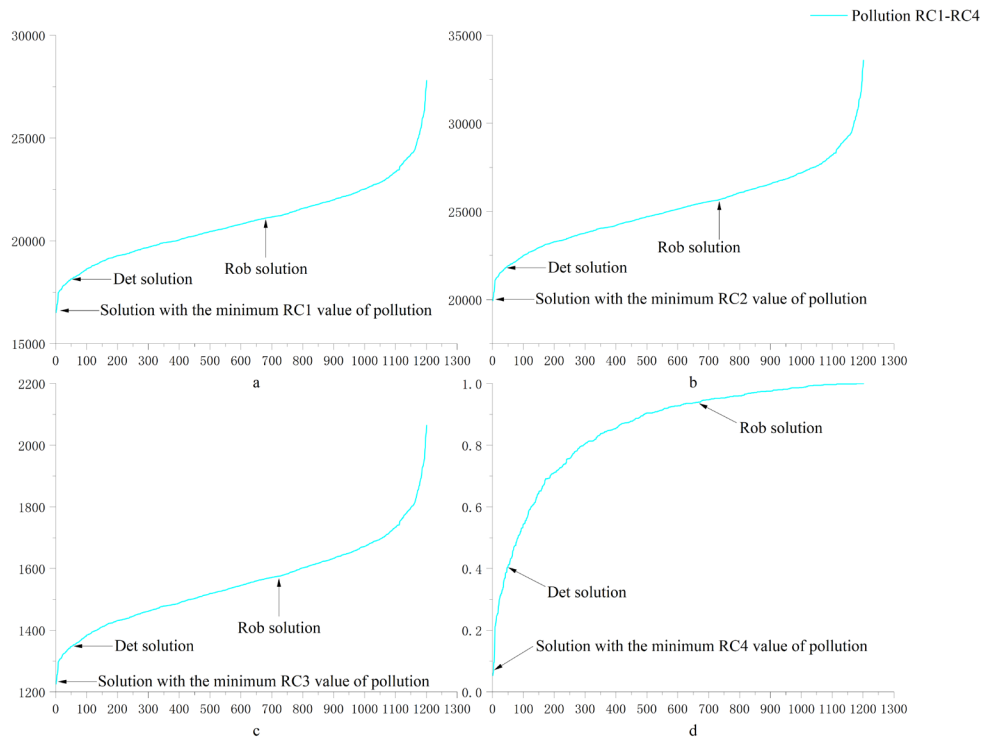
332 4.5 Comparing solutions found by deterministic and robust approaches

333 To see a more general relationship between the 1201 solutions (i.e., 1200 from the robust optimization
 334 solution and 1 from the deterministic optimization solution), the performance of each solution for water
 335 deficit and pollution on each of the four robustness criteria (sorted from smallest to largest) is plotted in
 336 Figure 8 and Figure 9.



337
 338 **Figure 8.** Robustness of water deficit (a: $RC1$, b: $RC2$, c: $RC3$, d: $RC4$). The horizontal coordinate
 339 represents the number of solutions and the vertical coordinate represents the robustness of the solution.

340
 341 As shown in Figure 8, for water scarcity, the robust solution performed significantly better than the
 342 deterministic solution. Specifically, for the four robustness criteria, the robust solution outperforms
 343 63.1%, 85.6%, 92.7%, and 77.7% of the solutions, respectively, while the deterministic solution
 344 outperforms only approximately 1% of the solutions. To analyze the robust and deterministic solutions
 345 more accurately and intuitively, this study applied the ratio of $RC(Det)/RC(Rob)$ to compare the
 346 robustness of the two solutions. The ratios of $RC(Det)/RC(Rob)$ are 1.53, 1.59, 2.62, and 12.67 in the
 347 four robustness criteria dimensions. This means that, regarding water deficit, the deterministic model
 348 solution may lead to 53%, 59%, 162%, and 1167% more variability in the four robustness criteria
 349 dimensions.

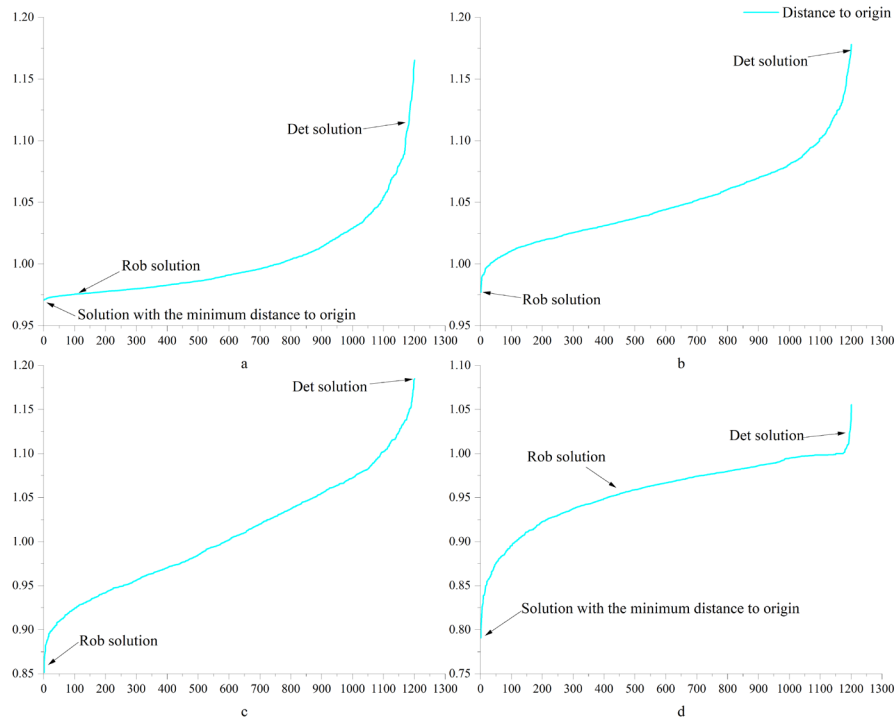


350

351 **Figure 9.** Robustness of pollution (a: $RC1$, b: $RC2$, c: $RC3$, d: $RC4$). The horizontal coordinate
 352 represents the number of solutions and the vertical coordinate represents the robustness of the solution.

353

354 However, as shown in Figure 9, the deterministic solution slightly outperforms the robust solution for
 355 pollution. Specifically, for the four robustness criteria, the deterministic solution outperforms 96% of the
 356 solutions, respectively, while the robust solution outperforms about 40% of the solutions. Similarly, we
 357 compare the two solutions by the ratio of $RC(Rob)/RC(Det)$. We find that the $RC(Rob)/RC(Det)$
 358 ratio is about 1.17 for $RC1$ to $RC3$ and 2.37 for $RC4$. This means that, in terms of pollution, the robust
 359 solution may lead to 17% more variability for $RC1$ to $RC3$ and 137% more variability for $RC4$.

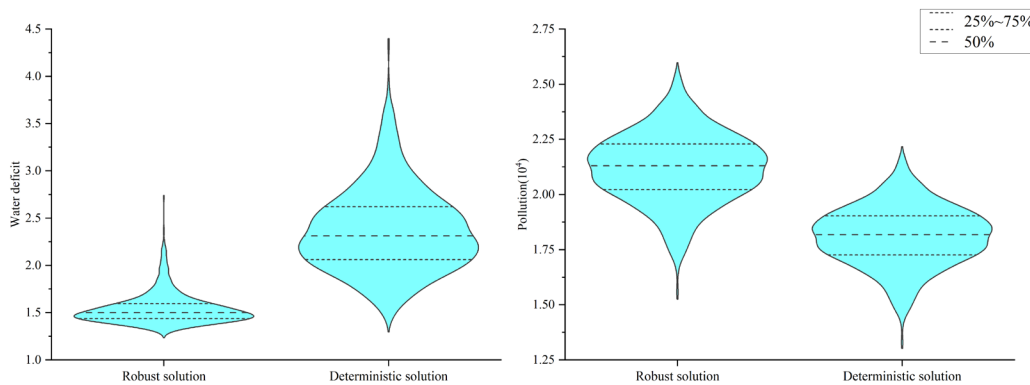


360

361 **Figure 10.** Comprehensive robustness for four indicators (a: $RC1$, b: $RC2$, c: $RC3$, d: $RC4$). The
 362 horizontal coordinate represents the number of solutions and the vertical coordinate represents the
 363 robustness of the solution.

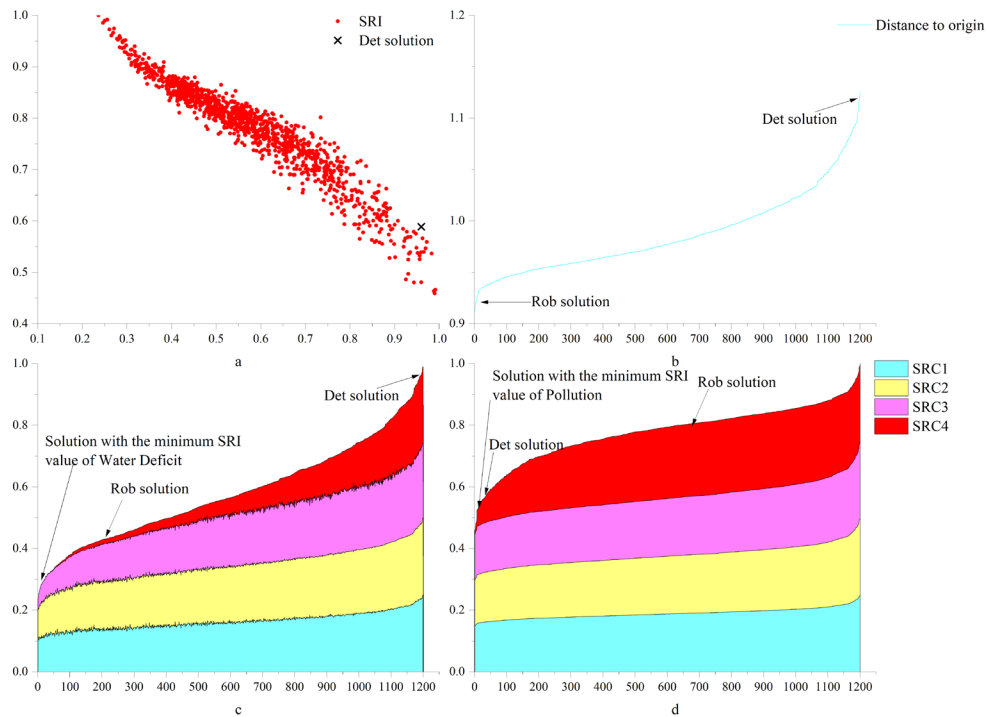
364

365 In order to analyze the comprehensive performance of each solution, rather than just the robustness of a
 366 single objective, this study reflects the comprehensive implementation of each solution in terms of the
 367 distance from the solution to the origin. As shown in Figure 10, the comprehensive performance of the
 368 robust solution for $RC1$ to $RC4$ is significantly better than that of the deterministic model solution.
 369 Specifically, the robust solution outperforms 90.3% and 62.2% of the solutions in $RC1$ and $RC4$,
 370 respectively, and outperforms all solutions in $RC2$ and $RC3$, while the deterministic solution performs
 371 exceptionally poorly in all four robustness criteria. According to the ratio of $Dis(Rob)/Dis(Det)$, we
 372 can find that the robust solution is 16.8%, 19.8%, 39.2%, and 7.3% more robust than the deterministic
 373 solution in the four robustness dimensions, respectively.



374

375 **Figure 11.** The integrated robustness index distribution of the robust and deterministic solution.



376

377 **Figure 12.** Comprehensive robustness criteria performance (a: Performance of comprehensive
 378 robustness criterion, b: Comprehensive robustness of robust solutions and deterministic solution, c and
 379 d: comprehensive robustness criteria for water deficit and pollution).

380

381 As shown in Figure 11, for water scarcity, the integrated criteria of the robust solution is clustered at
 382 approximately 0.5 and is significantly more robust than the deterministic solution; for pollution, the
 383 integrated index of the robust solution is significantly higher than that of the deterministic solution, but
 384 the span of the integrated index of the two solutions is similar, so the robustness of the deterministic
 385 solution is slightly better than that of the robust solution.

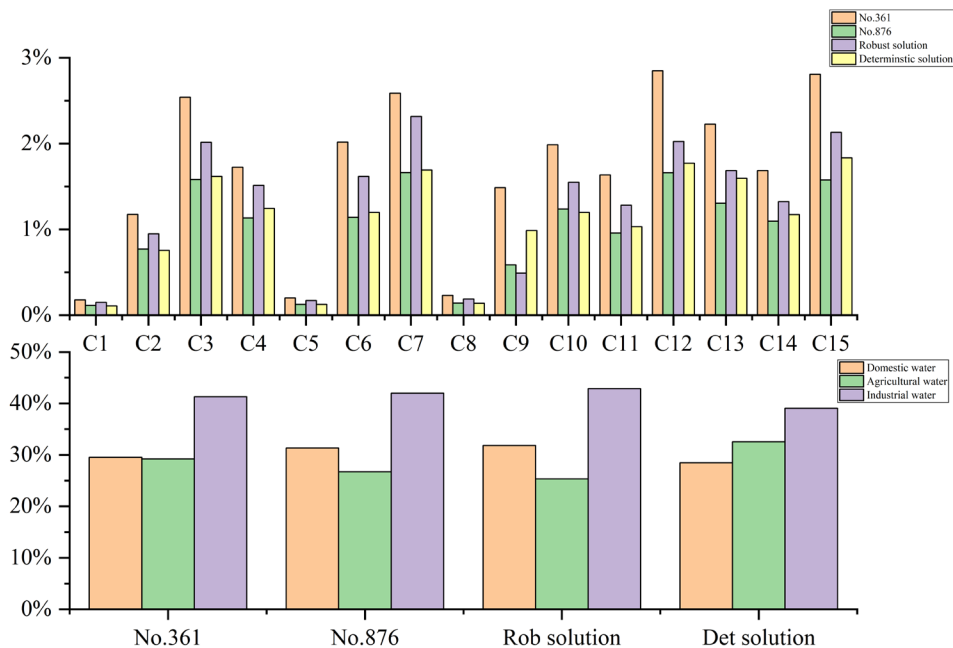
386 Similarly, as shown in Figure 12, there is also a Pareto front for the composite robustness criteria. For
 387 water deficit, the robustness of the robust solution is better than the deterministic solution; for pollution,
 388 the robustness of the deterministic solution is better than the robust solution. Specifically, for water deficit,
 389 the robust solution outperforms 85.3% of the solutions while the deterministic solution outperforms only
 390 about 1% of the solutions; for pollution, the deterministic solution outperforms 96% of the solutions
 391 while the robust solution outperforms only 39.6% of the solutions. According to the ratio of
 392 $SRI(Rob)/SRI(Det)$, the deterministic solution is about 130% more uncertain than the robust solution
 393 for water deficit; for pollution, the robust solution is about 37.7% more variable than the deterministic
 394 solution. The distance of each solution to the origin can reflect the comprehensive performance of the
 395 robustness of each solution. For the robustness composite index, the ratio of $Dis(Rob)/Dis(Det)$ is
 396 0.655, which means that the composite robustness of the robust solution is 52.6% higher than the
 397 robustness of the deterministic solution.

398 For the robustness composite, the robust solution outperforms all the solutions, while the deterministic
 399 model solution outperforms only about 3.2% of the solutions. Comparing the distance to the origin of
 400 the robust solution and the deterministic solution, we can find that the robustness of the robust solution
 401 improves by 27.8% over the deterministic solution.

402 **4.6 Analysis of specific water resources allocation schemes**

403 First, as shown in Figure 13, we analyzed the proportion of water supply for each city. We find that the
 404 water supply share for the scheme most robust to water deficit rates is significantly higher than that for
 405 the scheme with the most robust pollutant emissions. This is because an increase in water supply leads
 406 to an increase in pollutant emissions, which in turn leads to a decrease in the robustness of pollutant
 407 emissions. For specific cities, the least robust allocation scenario for water deficit reduces the water
 408 supply in City 3, City 7, City 10, City 12, and City 15 compared to the most robust allocation scenario
 409 for pollutant emissions. Interestingly, these cities have the most water demand in the basin (as shown in
 410 Figure 3). Therefore, basin managers can increase the water supply to these cities if they need to improve
 411 the water deficit robustness of the water resources allocation scheme.

412 Then we analyze specifically the distribution of water resources between sectors. An interesting
 413 phenomenon can be observed. As shown in Figure 13, although the scenario with the best robustness in
 414 terms of pollutant emissions has a lower water supply than the scenario with the best robustness in terms
 415 of water deficit, the reduction is mainly in the agricultural sector. Water for domestic and industrial
 416 production did not change much. The reason for this may be that agricultural water use causes more
 417 pollution and may create more uncertainty. So how can watershed managers hope that improving the
 418 robustness of pollutant discharge can reduce water supply to the agricultural sector.



419
 420 **Figure 13.** Specific water resources allocation schemes.

421 **5. Conclusion**

422 In this study, we propose a multi-objective robustness analysis method considering multiple uncertainties
 423 (CM-ROPAR approach) based on the robust optimization method for uncertainty perception (ROPAR
 424 approach). To verify the superiority and practicality of the CM-ROPAR approach, four robustness criteria
 425 are selected, and we compare the robust solution calculated by the method with the optimal solution of
 426 the deterministic model. In the studied case, there is a competitive relationship between the robustness
 427 of the two objective functions, which can form a Pareto frontier. For the water deficit rate, the robust
 428 solution outperforms the deterministic solution by 53%, 59%, 162%, and 1167% for the four robustness
 429 criteria, respectively; for the pollutant emission, the deterministic solution outperforms the robust

430 solution by only 17% for *RC1 – RC3*, and outperforms the robust solution by 137% for *RC4*. For the
431 composite robustness, the robust solution outperforms the deterministic solution by 52.6%, the CM-
432 ROPAR finds a more robust solution.

433 The CM-ROPAR approach permits to exhibit the handling of uncertainty, to be able to analyze how
434 uncertainty is transmitted to the Pareto frontier, and to perform the corresponding probabilistic analysis.
435 The novelty of the new method compared to existing ROPAR methods is reflected in two aspects. First,
436 the ROPAR method only considers uncertainty at a single point. In contrast, the CM-ROPAR method
437 considers multiple uncertainties through the joint probability distribution of two points, which is closer
438 to the actual situation and more general. Second, the new way analyzes the robustness of two objective
439 functions of the solution instead of fixing one objective function to analyze the robustness of the other
440 objective function. The CM-ROPAR method is more comprehensive and can identify the robustness of
441 both objective functions, giving decision-makers more information for decision making.

442 One of the limitations of this study is that the CM-ROPAR approach is applicable to problems with
443 two uncertainties and two objective functions; however, water allocation allows for more uncertainties
444 and more objective functions (e.g., the uncertainty of inflow between multiple tributaries). In future
445 research, we will focus on more complex objective functions and multi-objective optimization problems
446 with at least three objective functions.

447

448 *Author contribution.* JZ and DS conceptualized the study and wrote the paper. ZD provided the data. All
449 the authors took part in the interpretation of the results and edits of the paper.

450

451 *Competing interests.* The authors declare that they have no conflict of interest.

452

453 *Acknowledgements.* The authors are grateful to the Huaihe River Basin Management Committee for
454 providing valuable economic and hydrological data. The authors are also grateful to the insight and views
455 of the reviewers and editors. This research has been supported by Study on Multi-Objective Demand
456 Change and Regulation of Water Resources in North Jiangsu Province under Changing Situations
457 (105012014-2023-054) and the National key research and development program of China
458 (2016YFC0401306).

459

460 **Reference**

461 Abdalbaki, D., Al-Hindi, M., Yassine, A., and Abou Najm, M.: An optimization model for the
462 allocation of water resources, *Journal of Cleaner Production*, 164, 994-1006,
463 10.1016/j.jclepro.2017.07.024, 2017.

464 Ashofteh, P. S., Haddad, O. B., and A. Mariño, M.: Climate Change Impact on Reservoir
465 Performance Indexes in Agricultural Water Supply, *Journal of Irrigation and Drainage Engineering*,
466 139, 85-97, 10.1061/(asce)ir.1943-4774.0000496, 2013.

467 Beyer, H.-G. and Sendhoff, B.: Robust optimization – A comprehensive survey, *Computer Methods*
468 *in Applied Mechanics and Engineering*, 196, 3190-3218, 10.1016/j.cma.2007.03.003, 2007.

469 Chen, L., Xu, L., and Yang, Z.: Accounting carbon emission changes under regional industrial
470 transfer in an urban agglomeration in China's Pearl River Delta, *Journal of Cleaner Production*, 167,
471 110-119, 10.1016/j.jclepro.2017.08.041, 2017.

472 Dong, Y. and Xu, L.: Aggregate risk of reactive nitrogen under anthropogenic disturbance in the
473 Pearl River Delta urban agglomeration, *Journal of Cleaner Production*, 211, 490-502,

474 10.1016/j.jclepro.2018.11.194, 2019.

475 Habibi Davijani, M., Banihabib, M. E., Nadjafzadeh Anvar, A., and Hashemi, S. R.: Multi-Objective
476 Optimization Model for the Allocation of Water Resources in Arid Regions Based on the
477 Maximization of Socioeconomic Efficiency, *Water Resources Management*, 30, 927-946,
478 10.1007/s11269-015-1200-y, 2016.

479 Hassanzadeh, E., Elshorbagy, A., Wheeler, H., and Gober, P.: A risk-based framework for water
480 resource management under changing water availability, policy options, and irrigation expansion,
481 *Advances in Water Resources*, 94, 291-306, 10.1016/j.adwatres.2016.05.018, 2016.

482 Jin, S. W., Li, Y. P., Yu, L., Suo, C., and Zhang, K.: Multidivisional planning model for energy, water
483 and environment considering synergies, trade-offs and uncertainty, *Journal of Cleaner Production*,
484 259, 10.1016/j.jclepro.2020.121070, 2020.

485 Kang, D. and Lansley, K.: Scenario-Based Robust Optimization of Regional Water and Wastewater
486 Infrastructure, *Journal of Water Resources Planning and Management*, 139, 325-338,
487 10.1061/(asce)wr.1943-5452.0000236, 2013.

488 Kapelan, Z., Savic, D. A., Walters, G. A., and Babayan, A. V.: Risk- and robustness-based solutions
489 to a multi-objective water distribution system rehabilitation problem under uncertainty, *Water Sci
490 Technol*, 53, 61-75, 10.2166/wst.2006.008, 2006.

491 Kapelan, Z. S., Savic, D. A., and Walters, G. A.: Multiobjective design of water distribution systems
492 under uncertainty, *Water Resources Research*, 41, 10.1029/2004wr003787, 2005.

493 Keath, N. A. and Brown, R. R.: Extreme events: being prepared for the pitfalls with progressing
494 sustainable urban water management, *Water Sci Technol*, 59, 1271-1280, 10.2166/wst.2009.136,
495 2009.

496 Li, M., Fu, Q., Singh, V. P., Liu, D., and Gong, X.: Risk-based agricultural water allocation under
497 multiple uncertainties, *Agricultural Water Management*, 233, 10.1016/j.agwat.2020.106105, 2020.

498 Lu, H., Ren, L., Chen, Y., Tian, P., and Liu, J.: A cloud model based multi-attribute decision making
499 approach for selection and evaluation of groundwater management schemes, *Journal of
500 Hydrology*, 555, 881-893, 10.1016/j.jhydrol.2017.10.009, 2017.

501 Ma, Y., Li, Y. P., and Huang, G. H.: A bi-level chance-constrained programming method for
502 quantifying the effectiveness of water-trading to water-food-ecology nexus in Amu Darya River
503 basin of Central Asia, *Environ Res*, 183, 109229, 10.1016/j.envres.2020.109229, 2020.

504 Marchi, A., Dandy, G. C., and Maier, H. R.: Integrated Approach for Optimizing the Design of
505 Aquifer Storage and Recovery Stormwater Harvesting Schemes Accounting for Externalities and
506 Climate Change, *Journal of Water Resources Planning and Management*, 142,
507 10.1061/(asce)wr.1943-5452.0000628, 2016.

508 Marquez Calvo, O. O., Quintiliani, C., Alfonso, L., Di Cristo, C., Leopardi, A., Solomatine, D., and de
509 Marinis, G.: Robust optimization of valve management to improve water quality in WDNs under
510 demand uncertainty, *Urban Water Journal*, 15, 943-952, 10.1080/1573062x.2019.1595673, 2019.

511 Nelsen, R. B., Quesada-Molina, J. J., Rodríguez-Lallena, J. A., and Úbeda-Flores, M.: On the
512 construction of copulas and quasi-copulas with given diagonal sections, *Insurance: Mathematics
513 and Economics*, 42, 473-483, 10.1016/j.insmatheco.2006.11.011, 2008.

514 Nikoo, M. R., Kerachian, R., Karimi, A., and Azadnia, A. A.: Optimal water and waste-load allocations
515 in rivers using a fuzzy transformation technique: a case study, *Environ Monit Assess*, 185, 2483-
516 2502, 10.1007/s10661-012-2726-6, 2013.

517 Quintiliani, C., Marquez-Calvo, O., Alfonso, L., Di Cristo, C., Leopardi, A., Solomatine, D. P., and de

518 Marinis, G.: Multiobjective Valve Management Optimization Formulations for Water Quality
519 Enhancement in Water Distribution Networks, *Journal of Water Resources Planning and*
520 *Management*, 145, 10.1061/(asce)wr.1943-5452.0001133, 2019.

521 Reed, P. M., Hadka, D., Herman, J. D., Kasprzyk, J. R., and Kollat, J. B.: Evolutionary multiobjective
522 optimization in water resources: The past, present, and future, *Advances in Water Resources*, 51,
523 438-456, 10.1016/j.advwatres.2012.01.005, 2013.

524 Ren, C., Li, Z., and Zhang, H.: Integrated multi-objective stochastic fuzzy programming and AHP
525 method for agricultural water and land optimization allocation under multiple uncertainties,
526 *Journal of Cleaner Production*, 210, 12-24, 10.1016/j.jclepro.2018.10.348, 2019.

527 Salvadori, G., Michele, C. D., Kottegoda, N. T., and Rosso, R.: *Extremes in Nature: An Approach*
528 *Using Copulas*, *Extremes in Nature: An Approach Using Copulas*, By G. Salvadori, C. De Michele,
529 N.T. Kottegoda, and R. Rosso. Berlin: Springer, 2007., 2007.

530 Solomatine, D.: An approach to multi-objective robust optimization allowing for explicit analysis
531 of robustness, <https://www.un-ihe.org/sites/default/files/solomatine-ropar.pdf>, 2012.

532 Solomatine, D. P. and Marquez-Calvo, O. O.: Approach to robust multi-objective optimization and
533 probabilistic analysis: the ROPAR algorithm, *Journal of Hydroinformatics*, 21, 427-440,
534 10.2166/hydro.2019.095, 2019.

535 Sun, S., Fu, G., Bao, C., and Fang, C.: Identifying hydro-climatic and socioeconomic forces of water
536 scarcity through structural decomposition analysis: A case study of Beijing city, *Sci Total Environ*,
537 687, 590-600, 10.1016/j.scitotenv.2019.06.143, 2019.

538 Xiong, W., Li, Y., Pfister, S., Zhang, W., Wang, C., and Wang, P.: Improving water ecosystem
539 sustainability of urban water system by management strategies optimization, *J Environ Manage*,
540 254, 109766, 10.1016/j.jenvman.2019.109766, 2020.

541 Xu, Z., Pan, B., Han, M., Zhu, J., and Tian, L.: Spatial-temporal distribution of rainfall erosivity,
542 erosivity density and correlation with El Niño-Southern Oscillation in the Huaihe River Basin, China,
543 *Ecological Informatics*, 52, 14-25, 10.1016/j.ecoinf.2019.04.004, 2019.

544 Yang, W., Li, X., Sun, T., Pei, J., and Li, M.: Macroinvertebrate functional groups as indicators of
545 ecological restoration in the northern part of China's Yellow River Delta Wetlands, *Ecological*
546 *Indicators*, 82, 381-391, 10.1016/j.ecolind.2017.06.057, 2017.

547 Yazdi, J., Lee, E. H., and Kim, J. H.: Stochastic Multiobjective Optimization Model for Urban Drainage
548 Network Rehabilitation, *Journal of Water Resources Planning and Management*, 141,
549 10.1061/(asce)wr.1943-5452.0000491, 2015.

550 Yu, S. and Lu, H.: An integrated model of water resources optimization allocation based on
551 projection pursuit model – Grey wolf optimization method in a transboundary river basin, *Journal*
552 *of Hydrology*, 559, 156-165, 10.1016/j.jhydrol.2018.02.033, 2018.

553 Zeng, X., Zhao, J., Wang, D., Kong, X., Zhu, Y., Liu, Z., Dai, W., and Huang, G.: Scenario analysis of
554 a sustainable water-food nexus optimization with consideration of population-economy
555 regulation in Beijing-Tianjin-Hebei region, *Journal of Cleaner Production*, 228, 927-940,
556 10.1016/j.jclepro.2019.04.319, 2019.

557 Zhu, F., Zhong, P.-a., Cao, Q., Chen, J., Sun, Y., and Fu, J.: A stochastic multi-criteria decision making
558 framework for robust water resources management under uncertainty, *Journal of Hydrology*, 576,
559 287-298, 10.1016/j.jhydrol.2019.06.049, 2019.

560 Zhuang, X. W., Li, Y. P., Nie, S., Fan, Y. R., and Huang, G. H.: Analyzing climate change impacts on
561 water resources under uncertainty using an integrated simulation-optimization approach, *Journal*

562 of Hydrology, 556, 523-538, 10.1016/j.jhydrol.2017.11.016, 2018.
563